Soft Matter

PAPER

View Article Online
View Journal

Cite this: DOI: 10.1039/d5sm00298b

Influence of polymer architecture, ionization, and salt annealing on the stiffness of weak polyelectrolyte multilayers†

Jordan Brito,[a] Annie Luse,[b] Aliaksei Aliakseyeu[c] and Svetlana A. Sukhishvili *[a]

The layer-by-layer deposition of polyelectrolyte multilayers (PEMs) is a versatile and widely used technique of forming nanoscale polymer films with controlled properties. Yet, the influence of polymer architecture and assembly conditions on the mechanical properties of PEM films is not well understood. In this paper, we compare the growth and mechanical properties of all-linear PEM films *versus* all-star (8-arm) PEM films assembled at varied assembly pH. The properties of these PEM systems, composed of linear and 8-arm weak polyelectrolytes poly(2-aminoethyl methacrylate) (PAMA) and poly(methacrylic acid) (PMAA), are affected by the assembly pH, leading to differences in internal ionization, film growth rates, swelling, and Young's modulus. For films assembled using either linear or star polyelectrolytes in acidic conditions – where PMAA has low ionization – we show slow, linear growth with reduced swelling and similar Young's moduli of the as-deposited PEM films. However, a striking difference in the mechanical behavior of dry PEM films made from linear and star polymers was found for the films showing nonlinear growth (*i.e.*, assembled at neutral and slightly alkaline conditions). Specifically, while all-star films demonstrated relatively high, thickness-independent Young's moduli, the stiffness of all-linear PEM films strongly decreased with film thickness, reflecting the overall weakening of the network of ionic connections. Finally, we show that the ductility of all-star films was more affected by salt annealing than all-linear films, which agrees with previous reports of faster salt-induced diffusion of polyelectrolytes in PEM films composed of star polymers.

Received 21st March 2025,
Accepted 23rd June 2025

DOI: 10.1039/d5sm00298b

rsc.li/soft-matter-journal

Introduction

Polyelectrolyte multilayers (PEMs) have emerged as a significant class of polymer coatings with a broad range of applications, including bioactive delivery vehicles, separation membranes, biosensing devices, and coatings to modulate biological-surface interactions.[1–9] Composed of alternating layers of polyanions and polycations, PEMs exhibit a distinct combination of mechanical and chemical properties that can be finely tuned through various methods, such as polyanion/polycation binding strength,[10–12] assembly pH,[13] salt type/concentration,[14–16] temperature,[17] post-deposition annealing conditions,[18,19] and other environmental stimuli.[20] Due to the nanoscale thicknesses of PEMs, their mechanical stiffness, quantified by Young's modulus, is not commonly reported and remains poorly understood. Understanding correlations between molecular properties (such as chemical makeup, molecular architecture, and charge density), intermolecular binding, and mechanical properties of PEMs as deposited and after exposure to environmental stimuli (*e.g.*, biological conditions) is essential for designing their properties for targeted applications.

A variety of techniques have been used to measure the mechanical properties of thin polymer films, including atomic force microscopy (AFM), strain-induced elastic buckling instability for mechanical measurements (SIEBIMM), and most commonly, nanoindentation. Multiple studies of mechanical properties of PEMs composed of linear polyelectrolytes used nanoindentation to explore the effect of assembly pH on the Young's modulus of the films.[21–23] These prior studies were

[a] *Department of Materials Science & Engineering, Texas A&M University, College Station, Texas 77843, USA. E-mail: svetlana@tamu.edu*
[b] *Department of Physics and Astronomy, Texas A&M University, College Station, Texas 77843, USA*
[c] *Artie McFerrin Department of Chemical Engineering, Texas A&M University, College Station, Texas 77843, USA*

† Electronic supplementary information (ESI) available: Procedural details of image analysis, error propagation, bilayer thicknesses, linear regression of PEM growth rates, individual layer thicknesses, PAMA percentage in the films, infrared spectra of individual components, deconvoluted infrared spectra of as-deposited PEM films, water content in the as-deposited PEM films, effect of strain rate on buckling wavelength, and infrared spectra, change of thickness, and optical images of wrinkling of PEM films before and after salt exposure. See DOI: https://doi.org/10.1039/d5sm00298b

performed with multilayers of poly(allylamine hydrochloride) (PAH) and poly(acrylic acid) (PAA) having solution pK_a ~9 and ~4.5, respectively, assembled from pH 2, 4, and 6.5.[21] The highest Young's modulus of ~150 MPa was reported for PAH/PAA PEMs assembled from pH 6.5, where both polyelectrolytes were highly charged and grew the slowest. In contrast, the faster growing PAH/PAA films assembled from pH 2, where PAA had a low fraction of ionized groups, showed a Young's modulus over two orders of magnitude lower than PAH/PAA assembled from pH 6.5.[21] In another nanoindentation study of dry PAH/PAA PEMs exposed to ambient air, Young's modulus was in the GPa range, and assembly pH was also found to strongly affect PEM mechanical properties.[22] When PAH was assembled from pH 7.5 and PAA from pH 3.5, the charge on the polyelectrolytes and degree of ionic pairing were reduced, leading to thicker bilayers and a resulting lower hardness and Young's modulus compared to the films in which both PAH and PAA were assembled from the same pH (pH 6.5 or pH 3.5). This behavior was suggested to stem from the diffuse internal film structure, allowing easier deformation to accommodate the indenter tip.[22] A similar conclusion of the highest Young's modulus occurring in slow-growing PEMs at the highest overall ionization of the individual components was found using PAH with a carboxylated azobenzene-containing polyelectrolyte (P-Azo, pK_a ~3.3).[23] These studies related the observed trends mainly to strength of ionic pairing, showing that the slowest growth and highest Young's modulus occurred when both polyelectrolytes were highly charged with the highest degree of ionic pairing. Previously, our group used nanoindentation on nonionic, hydrogen-bonded films, correlating thin, linear film growth with stratified internal structure, lower swelling, and a high Young's modulus (~12 GPa) that did not change significantly in a wet state.[24]

Another way to explore mechanical properties of ultrathin polymer films is the SIEBIMM technique, which has also previously been employed for PEM films.[25,26] The SIEBIMM technique offers a precise method for evaluating the mechanical properties of thin films through differing elastic buckling of the polymer films and the substrate they are deposited on, typically polydimethylsiloxane (PDMS). In this technique, a low mechanical strain is applied to the coated PDMS inducing 'wrinkles' with measurable buckling wavelengths that are used to determine the Young's modulus of the thin film (see Materials and methods). The technique is particularly advantageous for PEMs over other mechanical measurement techniques, such as atomic force microscopy and nanoindentation, as these force-based techniques can give inflated Young's modulus values for thin films due to the proximity of the hard substrate.[27] Yet, for very thin films (sub-200-nm thick), propagation of error using the SIEBIMM technique may lead to high uncertainty below a specific ''cut-off'' point, primarily dictated by the standard deviation of the buckling wavelengths (see ESI†). In a previous report, this limit was set at ~80 nm,[27] but the cut-off of a specific system may change based on differing magnitude of Young's modulus, use of equipment with differing resolution, or nonuniformity of the samples. Still, the SIEBIMM technique allows compliance measurements of submicron films with high precision without requiring specialized equipment.[27–29] By analyzing the buckling patterns and the associated strain, we can understand how changes in ionization and molecular architecture influence the mechanical stiffness of PEMs.

Additionally, SIEBIMM allows the investigation of potential dependences of film thickness on the Young's modulus, not limited by penetration depth as in nanoindentation and AFM. While Young's modulus is fundamentally a thickness-independent material property for homogeneous materials, previous reports have shown that PEMs are not necessarily homogeneous throughout the film perpendicular to the surface of the substrate.[30] The PEMs can contain up to three zones of differing properties,[31] including a thin region near the substrate with slower diffusion, the bulk internal region, and a thin region near the film surface with faster diffusion.[30,32] Also, PEMs can change growth regimes from nonlinear to linear as a function of layer thickness,[33–35] leading to differences in the internal structure of the film. It is important to note that when using the SIEBIMM technique, the PEMs are treated as mechanically homogeneous materials throughout their entire thickness. Consequently, changes in Young's modulus for films of different thickness can reflect changes in the internal film structure in the direction perpendicular to the film surface.

Previously, the SIEBIMM technique was used for PAH/PAA PEMs assembled from pH 3.5, 4, and 7.5/3.5, with the authors reporting no significant effects of assembly pH on the overall Young's modulus (~9–10 GPa at 20% relative humidity).[29] However, for PEMs of thickness 60–300 nm assembled from pH 4 and 7.5/3.5, the authors reported a thickness-dependent Young's modulus, possibly due to different chain conformations due to substrate interactions.[29] This thickness dependence was also reported for PAH/poly(styrene sulfonate) (PSS) PEMs assembled from pH 3, highlighting the importance to measure Young's modulus values for PEMs at a range of thicknesses for reliable and accurate measurements.[27,29]

As described thus far, in the case of weak polyelectrolytes, the pH of the assembly solutions plays a key role in determining the electrostatic interactions between the layers, which in turn affects the mechanical properties of the multilayers. Previously, polyelectrolyte complexes containing star polyelectrolytes have been shown to have higher salt resistance, while having similar mechanical properties, as their linear counterparts.[36] Yet, to the best of our knowledge, all prior work on mechanical measurements of PEMs involved linear polyelectrolytes, while the role of molecular architecture on PEM stiffness remained unexplored. While linear polyelectrolytes have elongated chains that may form more ordered multilayer structures,[37] star polyelectrolytes, characterized by multiple arms radiating from a central core, present a unique case.[38] Unlike linear polyelectrolytes, star polyelectrolytes have a high degree of branching that leads to more interconnected networks within the multilayers and distinct physicochemical properties, such as uniform morphologies, enhanced stimuli-responsiveness, and higher diffusion rates.[37,39–41]

In previous works, our group laid down a foundation for the fundamental understanding of star polyelectrolyte behavior within PEMs and showed higher diffusion rates and higher salt sensitivity of star polyelectrolytes compared to linear counterparts within layer-by-layer assemblies.[40,42,43] However, correlations between the molecular structure, ionization of assembled polyelectrolytes, and mechanical properties of PEMs containing star polymers remained unexplored. In this paper, we use the SIEBIMM technique to compare the Young's modulus of films assembled from different assembly pH, influencing the degree of ionization of the weak polyelectrolytes–poly(2-aminoethyl methacrylate) (PAMA) and poly(methacrylic acid) (PMAA) – with differing polymer architecture (linear *vs.* 8-arm star polymer). We believe that the insights of this study can be used for tailoring mechanical properties of PEM materials for applications across a wide range of technological and industrial fields.

Results and discussion

Growth regimes and ionization of PAMA/PMAA multilayers

Linear and 8-arm star PAMA (LPAMA and SPAMA, respectively) were assembled with linear and 8-arm star PMAA (LPMAA and SPMAA, respectively) into PEMs, as shown in Fig. 1A, from solutions adjusted to a wide range of pH values (pH 3–11) to investigate the effect of ionization of the weak polyelectrolytes PAMA and PMAA on the growth of the PEMs. These linear and star polyelectrolytes were synthesized and characterized in our prior work,[43,44] and their molecular weights and number of units are provided in Fig. 1A. The linear and star counterparts (*i.e.*, LPAMA *vs.* SPAMA and LPMAA *vs.* SPMAA) had nearly matched molecular weights, only differing in number of arms. These molecular weights and number of arms were chosen to isolate the effects of polymer architecture on the resulting film properties. Furthermore, we selected the range of pH values from 3 to 11 to evaluate the full range of ionic pairing strength. Because the reported pK_a values for PAMA and PMAA in solution are 7.6[45,46] and 6–7,[14,47–49] respectively, and the effect of PEM environment on the pK_a of the assembled weak polyelectrolytes,[50] we expected to have reduced charge on PMAA below pH 5, reduced charge on PAMA above pH 8–9, and maximized charge on both PMAA and PAMA near pH 6–7. Fig. 1B shows that at pH 3 and 5 film growth was slower and more linear, whereas at pH 7 and pH 9 the films accumulated mass more rapidly and transitioned from nonlinear growth to linear growth after 4–6 bilayers. At pH 11, no growth occurred up to 8 bilayers, likely due to the drastically reduced charge on PAMA. As shown in Fig. 1A, PAMA has a lower molecular weight and about half the amount of monomer units than PMAA; this comparably reduced size can further contribute to the steep drop-off in growth observed between pH 9 and 11. In Fig. 1C, a clear maximum growth occurred at pH 7 with ~23 nm per bilayer, obtained from linear regression analysis within the linear regions of the growth curves. The slightly reduced growth rate at pH 9 as compared to pH 7 is due to some loss of charge on PAMA in the solution at pH 9. The linear growth regions were identified in Fig. S1 (ESI†) by a constant deposited thickness per bilayer, and occurred after 2 bilayers for pH 5, 4 bilayers for pH 7, and 6 bilayers for pH 9. The linear regressions for each assembly pH are provided in Fig. S2 (ESI†).

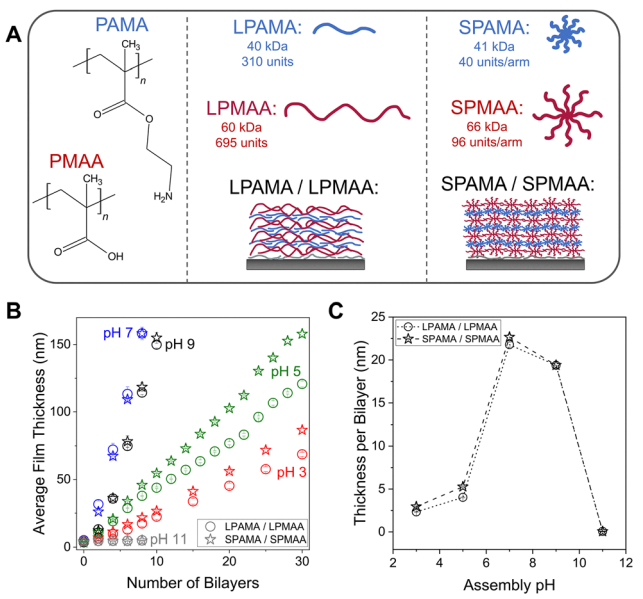

Fig. 1 (A) Chemical structures and schematics representing the components and assemblies of linear and star PAMA and PMAA LbL films. (B) Growth curves of PAMA/PMAA LbL films assembled at pH 3, 5, 7, 9, and 11, as measured by spectroscopic ellipsometry. Error bars are averaged from six measurements. (C) Growth per bilayer (*i.e.*, a single layer of PAMA with a single layer of PMAA) of the LbL films assembled at each pH. Thickness per bilayer values were obtained from linear regression analysis of the linear regions of each growth curve (see Fig. S1 and Fig. S2, ESI†).

The observed rapid growth near neutral pH (where ionization is the highest) is different than many reported linear PEM systems containing at least one weak polyelectrolyte (PAH/PSS,[12,51] PDADMAC/PAA,[12,52] PAH/PAA,[33,53,54] *etc.*) that show the most compact, thinnest growth at pH values where the charge density is maximized. Previously, Schlenoff *et al.* explored in detail how binding strength of polyelectrolyte complexes is affected by factors such as type of ionic functionality and hydrophilicity, and correlated loosely with water content.[55] In our case, while there are differences in the side group chemistry, hydrophobicity, and chain flexibility between PAMA/PMAA and the previously studied polyelectrolyte systems, one major difference between our PAMA/PMAA system and these previous systems is the gap between the pK_a values of the polycation and polyanion. In particular, the weak/weak polyelectrolyte system with PAH and PAA has pK_a values in bulk solution of ~8–9 and ~4.5,[21] respectively, exhibiting a wide gap of about 4 pH units before assembly, and allowing full ionization of both PAH and PAA in the range of pH 6 to 8 within the assembled films.[54] In contrast, the pK_a values of PAMA and PMAA (7.6 and 6–7)[14,45–49] have a gap of only about 1 pH unit, which likely reduces the range of expected "maximum" ionization to only around pH 7, with reduced ionization on PAMA or PMAA when deviating from neutral pH. Furthermore, film

growth rates of PEMs containing star polymers have exhibited more complex trends. For PAH/PAA assembled from pH 7.5, PEMs containing star PAA (32-arm) grew exponentially and faster than their linear counterparts, attributed to higher interlayer chain diffusion.[56] Similarly, in another study, poly(2-(dimethylamino)ethyl methacrylate) PDMAEMA (19-arm)/PAA (24-arm) were assembled from pH 6, and the all-star PEMs grew $\sim 3\times$ faster than the all-linear PEM.[41] Yet, for PDMAEMA (18-arm) and PAA (21-arm) with larger molecular weights assembled from pH 6, the differences in growth were less pronounced, with all-star films still experiencing exponential growth, albeit at a slightly slower pace compared to the all-linear films.[37]

In our system, we attribute the rapid growth near neutral pH to a higher diffusivity rate of the components within the highly charged film than in the likely kinetically trapped, non-equilibrated acidic assembly conditions. A similar behavior was previously reported for PDMAEMA/PMAA and PTMAEMA (fully quaternized PDMAEMA)/PMAA PEM systems and related to the kinetic stability of the components assembled as complexes in solution.[13] Similar to our work, the gap between the reported pK_a values of PDMAEMA and PMAA (6.7 and 6.5, respectively) is small. The film structure for PDMAEMA/PMAA PEMs, studied *via* neutron reflectometry, was shown to be completely intermixed for the exponentially growing PEMs and stratified for the PEMs displaying linear growth.[13] In our work, while complete intermixing may not occur as in the case of exponential films, we expect more diffuse layers at assembly pH 7 and 9 than those assembled at pH 3 and 5, represented schematically in Fig. 2 using star polyelectrolytes.

Using attenuated total reflectance Fourier transform infrared spectroscopy (ATR-FTIR), we then sought to explore differences in ionization of PMAA within the PEMs to relate to the mechanical properties of the film. Comparison of the infrared spectra of the PEMs with the individual components at pH 3 and pH 9 enabled identification (Fig. S4, ESI†) and deconvolution (Fig. S5 and S6, ESI†) of relevant peaks for the carbonyl groups in PAMA and PMAA. As discussed before, the reported pK_a values for PAMA and PMAA are 7.6 and 6–7 in solution, respectively,[14,45–49] but weak polyelectrolytes in PEMs are known to have shifted pK_a values with respect to their individual solution behavior due to induced charges.[49,54,57,58] In Fig. 3A, we show that the PMAA ionization trends of the PEMs have an apparent pK_a shifted to a lower pH, with 50% ionization near pH 5. Although we also expect a shift of the pK_a of PAMA (*i.e.*, an increase from its solution value of 7.6) within the multilayers, quantification of the ionization of PAMA within the films proved difficult due to the low intensity of these peaks compared to PMAA, along with spectral overlap in the 1600 cm^{-1} (N–H bending vibrations due to primary amines NH_2) and 1520 cm^{-1} (N–H bending due to NH_3^+) regions. Additionally, the PEMs assembled from acidic solutions (pH 3 and 5, Fig. S5 and S6, ESI†) show larger peaks for hydrogen-bonded COOH dimers between/within the PMAA chains than those assembled at pH 7 and 9. These trends for hydrogen bonding at lower pH values and higher ionization of PMAA at higher pH values are represented schematically in Fig. 3B.[59,60] Finally, analysis of the water bending peak at 1640 cm^{-1} allowed for comparison of the relative water content for each assembly pH, showing that the films assembled from acidic pH, where hydrogen bonding is stronger and more prevalent, contained less water than those assembled at pH 7 and 9 (Fig. S7, ESI†).

While the pH dependence of PMAA ionization and the overall mass per bilayer, and thus the density of ionic pairing, appeared to be similar for linear and star films, we then investigated whether molecular architecture alone could influence the mechanical properties of the films.

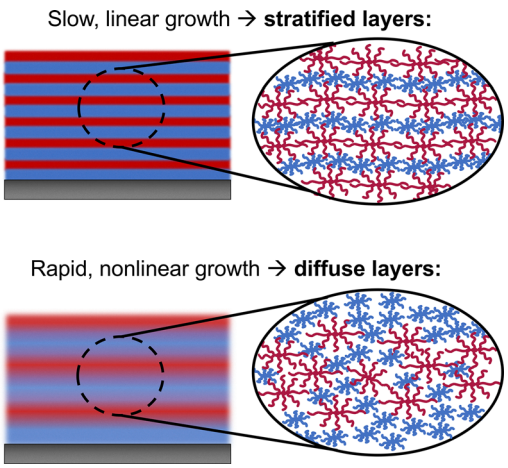

Fig. 2 Graphic representation of slow growing SPAMA/SPMAA films with stratified layers and rapid growing SPAMA/SPMAA films with diffuse layers.

Young's modulus of as-deposited PAMA/PMAA PEM films

To determine the Young's modulus of the dry PAMA/PMAA PEMs, films of different thicknesses were deposited on PDMS substrates and subjected to uniaxial tensile force to create visible wrinkles on the surface, which were then observed under optical microscopy. Using the SIEBIMM technique, the Young's modulus of each PEM film was calculated based on the thickness of the PEM film, as measured by spectroscopic ellipsometry, and the resulting buckling wavelength of the wrinkles, as measured by image analysis of optical micrographs. In-depth procedural details of the image analysis are provided in the ESI.† As mentioned before, it is important to remember that the SIEBIMM technique assumes homogeneity throughout the PEM film, measuring an average modulus that can mask the variations of mechanical properties across the film thickness.

In Fig. 4, the buckling wavelengths of all PEM films are plotted against dry film thickness. All mechanical measurements were taken in similar ambient conditions, ranging from 54–57% relative humidity and 20.8–21.6 °C. Changes in the environmental conditions, particularly humidity, have been shown to affect the Young's modulus of PEMs previously.[61] However, the minor changes in the recorded humidity and temperature during our measurements are unlikely to have

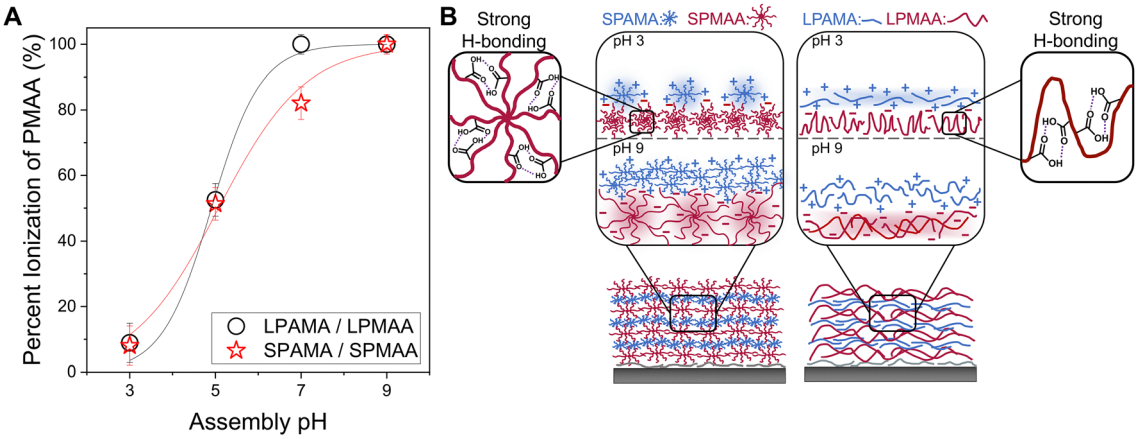

Fig. 3 (A) Percent ionization of PMAA groups with the LbL films assembled at pH 3, 5, 7, and 9, as determined by deconvolution of infrared spectra collected *via* ATR-FTIR spectroscopy. All PEM films had LPMAA or SPMAA as the top layer. Error bars were calculated based on the quality of the fits of the deconvoluted peaks. (B) Schematics showing the changes of ionization in films assembled from acidic *versus* basic pH. Insets show a high degree of hydrogen bonding and low ionization of PMAA in films assembled in acidic conditions.

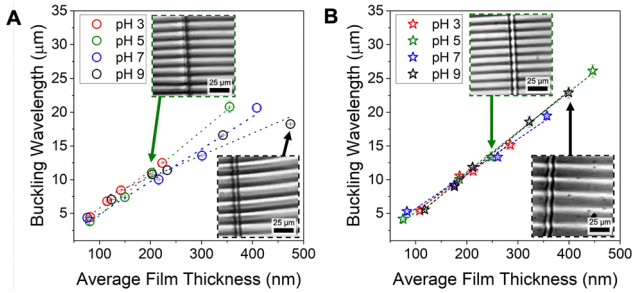

Fig. 4 Buckling wavelength of all LPAMA/LPMAA (A) and SPAMA/SPMAA (B) PEM films assembled from pH 3, 5, 7, and 9. Dashed linear trendlines are shown in all panels to guide the eye. Inset images show examples of wrinkles for pH 5 and pH 9 films, with a scale bar of 25 μm. The R^2 values of the linear trendlines for panel A are 0.993 (pH 3), 0.998 (pH 5), 0.982 (pH 7), and 0.946 (pH 9). For panel B, the R^2 values are 0.989 (pH 3), 0.997 (pH 5), 0.991 (pH 7), and 0.998 (pH 9).

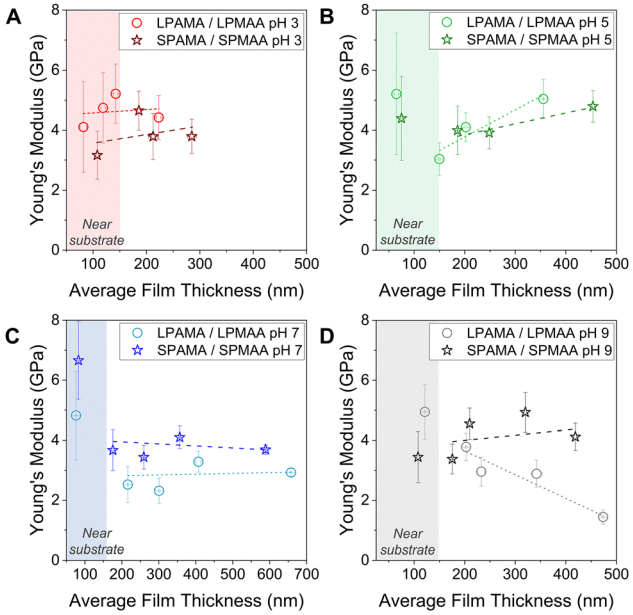

Fig. 5 Young's modulus of LPAMA/LPMAA and SPAMA/SPMAA PEM films deposited from pH 3 (A), pH 5 (B), pH 7 (C), and pH 9 (D). Dashed linear trendlines are shown in all panels. The shaded areas indicate the measurements of thin (<150 nm) PEM films which showed the strongest scatter. The error bars on all data points were calculated according to the propagation of error analysis detailed in the ESI.†

significant effects. Also, as shown in Fig. S8 (ESI†), the strain rate did not appear to influence the buckling wavelength in these measurements, with strain rates of 5×10^{-4} s^{-1} yielding similar buckling wavelengths as 2.5×10^{-4} s^{-1} and stationary measurements after wrinkles were formed.

Fig. 4A and B illustrate that the buckling wavelength exhibited distinct variations in relation to film thickness between LPAMA/LPMAA and SPAMA/SPMAA films. The linear trendlines of the buckling wavelengths for LPAMA/LPMAA PEMs show lower R^2 with increasing assembly pH, indicating a greater thickness dependence at higher pH (Fig. 4A). In contrast, in star-containing films (Fig. 4B), the consistently high R^2 values and overlap of the buckling wavelengths for each assembly pH suggest that the Young's modulus remains relatively constant, irrespective of the film thickness or assembly pH.

The Young's modulus values for all as-deposited PEMs (E_f), calculated from the buckling wavelengths in Fig. 4, are shown in Fig. 5. In these Figures, the range of film thicknesses below ~150 nm is shaded due to high error. Because E_f is on the order of $(\lambda/d_f)^3$, where λ is the buckling wavelength in micrometers and d_f is the film thickness in nanometers, the propagation of error for thin films is significant. The detailed analysis of this propagation of error is provided in the ESI.† The high error for thin films is in line with the previous report that the accuracy of SIEBIMM is limited by the thickness of the PEM film on PDMS (>70 nm),[27] although it is still more accurate at lower thicknesses than nanoindentation (often requiring micron-thick samples). Additionally, the proximity of the substrate to the film surface in this near-substrate thickness range

may influence the apparent compliance of the film.[27] Therefore, in our work, the Young's modulus of films with thicknesses below approximately 150 nm has not been further explored and the data points in this range are excluded from linear regression for pH 5, 7, and 9.

Comparison of films with thicknesses greater than 150 nm shows that at pH 3 (Fig. 5A) and 5 (Fig. 5B), the Young's modulus values of LPAMA/LPMAA and SPAMA/SPMAA were similar at about 4–5 GPa, suggesting that the thin stratified layers interact strongly and similarly between the linear and star systems. At these conditions, the hydrogen bonding occurring from acidic assembly conditions (Fig. 3B) can also help strengthen the films. Also, as shown in Fig. S7 (ESI†), the PEMs assembled from pH 3 and pH 5 contained less water than those assembled at pH 7 and 9, likely strengthening the film. The linear and star PEMs assembled at pH 5 showed relatively low swelling ratios (~150% of original thickness) that were independent of the original film thickness when exposed to phosphate buffer solution at matched pH as assembly (Fig. 6A), further highlighting a lack of thickness dependence at assembly pH 5. In these swelling experiments, the PAMA/PMAA films of differing thickness were exposed to 0.01 M phosphate buffer that was pH adjusted to match the assembly conditions of the PEMs, and the change in thickness of the films were measured over time *via in situ* spectroscopic ellipsometry until the film thickness plateaued, indicating that the film was fully swollen. The swelling ratio was calculated from the initial dry thickness and the fully swollen thickness. Phosphate buffer was selected in both the assembly and swelling of PEM films to maintain constant pH with constant low ionic strength.

The modulus values for pH 3 and 5 PAMA/PMAA assemblies are also on the same scale as those obtained in previous work conducted by Nolte *et al.*[27] using SIEBIMM for PEMs of weak/strong linear polyelectrolytes PAH/PSS at pH 2. In their study, both PAH and PSS were assumed to be fully charged. The PAH/PSS PEMs grew at a rate of approximately 2 nm per bilayer and had a modulus value of 5 to 6 GPa.[27] These values are comparable to the growth rate and modulus values of PAMA/PMAA PEMs that were assembled at pH 3 and 5 in this work (~3–5 nm per bilayer, 4–5 GPa), although PMAA ionization in this case is expected to be the lowest.

However, for assembly pH 7 and 9 (Fig. 5C and D) where the PEM growth was rapid and nonlinear, we observed notable differences in the magnitude and, for pH 9 specifically, thickness dependence of the Young's modulus between the linear and star PEMs with thicknesses greater than 150 nm. The most striking result is the high value of Young's modulus of SPAMA/SPMAA PEMs (4–5 GPa) assembled at pH 9 compared to LPAMA/LPMAA PEMs (2–4 GPa). A similar result, although less stark, was observed for the films assembled at pH 7, where star-containing films also showed a higher Young's moduli than LPAMA/LPMAA films (4 GPa *versus* 2.5 GPa). The linear and star PEMs assembled at pH 7 also showed swelling ratios that were independent of the film thickness, with star PEMs swelling slightly less than the linear PEMs (Fig. 6B).

Another distinction is that the Young's modulus and swelling ratios of SPAMA/SPMAA PEMs across all tested pH values remained independent of film thickness, while the LPAMA/LPMAA PEMs assembled from pH 9 exhibit a distinct thickness dependence, showing a decrease in Young's modulus from 5 GPa to 1 GPa for films approximately 500 nm thick. This behavior in the pH 9 films that displayed nonlinear, rapid growth was further investigated with *in situ* swelling experiments (Fig. 6C), showing that the swelling ratio of all-linear films increased significantly with original film thickness (from 140% at 100 nm to 230% at 350 nm), while the swelling ratios of all-star films again remained constant with thickness (~170%). The high swelling of PEM films at pH 9 is likely related to the mismatch in PAMA/PMAA charge densities stemming from the assembly pH. As shown in Fig. S3 (ESI†), FTIR analysis indicated an increase in the ratio of PAMA within the films with the increase of assembly pH, resulting in the highest ratio of PAMA at pH 9.

To determine the cause of the decrease in Young's modulus and increase in swelling for thicker all-linear pH 9 films, we compared the FTIR spectra of thin films (~150 nm) to thicker films (~350 nm) to see if the ratio of PAMA changes with film thickness (Fig. S9, ESI†). Since there were no statistically significant differences with film thickness, we believe the thickness-dependent Young's modulus and swelling of linear films assembled from pH 9 can be explained by the difference in the molecular film layering in regions near the surface, near

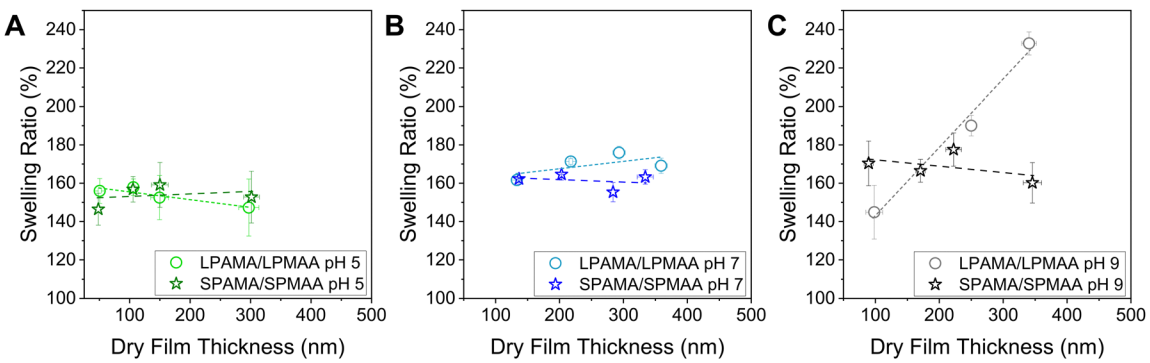

Fig. 6 Swelling ratios of LPAMA/LPMAA and SPAMA/SPMAA PEM films deposited from pH 5 (A), pH 7 (B), and pH 9 (C). Dashed linear trendlines are shown in all panels.

the substrate, and in the bulk, and differing growth regimes with film thickness. Specifically, previous neutron reflectometry studies have shown that films are more stratified near the substrate and become increasingly intermixed farther away, even in the case of linearly-growing films.[62,63] The weak binding of polyelectrolyte chains due to the reduced ionization of PAMA at pH 9 further favors such chain intermixing and the larger film swelling of thicker all-linear films at this pH (Fig. 6C). In contrast to linear chains, star molecules are more compact, have higher local unit density, and are more rigid, resulting in SPAMA/SPMAA binding that resists excessive swelling.

Altogether, the above results indicate that all-star films are more robust, demonstrating thickness- and pH-independent swelling and Young's modulus, and are stronger than all-linear PEMs at high pH. Our results indicate that weak star polyelectrolytes interact in a more uniform bulk spatial distribution within a wide pH range, even within the thicker films which involve significant molecular interdiffusion. These results add on to the prior studies of Young's modulus for weak linear PEMs (*e.g.*, PAH/PAA),[22,29] which correlated Young's moduli mainly with ionic pairing. Here, we show that in addition to ionic pairing, molecular architecture plays a critical role in defining mechanical properties of PEMs. Specifically, we suggest that the Young's modulus of PEMs is not solely determined by the extent of ionic pairing but also by the connectivity and topology of the network formed through ionic and covalent interactions, which can be tuned by the molecular architecture and assembly conditions.

Mechanical properties of LPAMA/LPMAA and SPAMA/SPMAA PEM films after salt annealing

So far, we have shown that as-deposited PEMs containing star polyelectrolytes have more uniform mechanical properties than their linear counterparts based on their pH-independent Young's modulus values. Next, based on our previous work on the salt-induced diffusion of star and linear polymers in PEMs, we aimed to explore how polymer architecture affects the mechanical properties after salt annealing. To achieve this, we exposed the as-deposited PEMs to 0.5 M NaCl solutions at matched pH as assembly and measured the remaining thickness to assess salt stability. All PEM films assembled from pH 5, 7, and 9 remained at the surface after salt exposure with negligible changes in thickness (Fig. S10, ESI†). However, PEMs assembled from pH 3 were not used for mechanical testing after salt exposure due to delamination of the LPAMA/LPMAA PEMs. The addition of salt to the LPAMA/LPMAA films assembled from pH 3 likely weakened the low amount of ionic pairing within the film, leading to delamination. The higher stability of salt-annealed SPAMA/SPMAA films assembled from pH 3 is consistent with previous reports of star-based polyelectrolyte complexes in solution, which showed higher stability in salt conditions than their linear counterparts.[36] The infrared spectra of the PEMs (Fig. S11, ESI†) showed a slight decrease in PMAA ionization after salt exposure, which was more significant for LPAMA/LPMAA PEMs, consistent with previous reports of salt screening on ionic pairs and resulting protonation of carboxylic acid groups.[42]

However, as shown in Fig. 7A, when applying stress to the salt-annealed PEMs, the critical wrinkle strain was much larger (>10%) for all samples, except LPAMA/LPMAA pH 5, than the as-deposited PEMs (~3% strain). The critical wrinkle strain refers to the applied tensile strain at which sufficient wrinkling occurs, in our case often associated with formation of cracks in the film, with higher values indicating greater film ductility.[26] Furthermore, the induced wrinkles at high strain on both pH 9 samples and the SPAMA/SPMAA pH 5 sample had a wider range of wavelengths after salt annealing (Fig. S12, ESI†), making

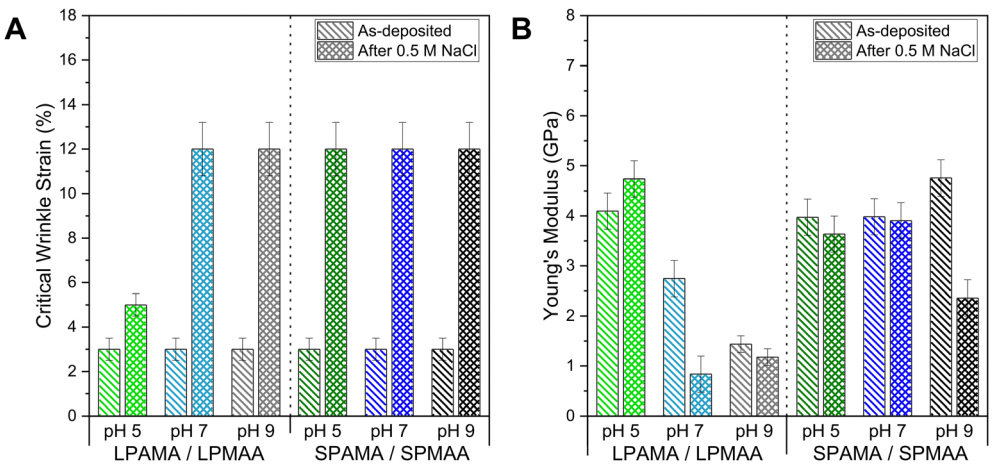

Fig. 7 Critical wrinkle strain (A) and Young's modulus values (B) for LPAMA/LPMAA and SPAMA/SPMAA multilayer films deposited from pH 5 (green bars), pH 7 (blue bars), and pH 9 (black bars) solutions before and after being exposed to 0.5 M NaCl solutions at matched pH for 30 min, rinsed in 0.01 phosphate buffer at matched pH, and dried under a flow of nitrogen gas. The thickness of the samples used for the pH 5 data were ~200 nm for LPAMA/LPMAA and ~250 nm for SPAMA/SPMAA. The thickness of the samples used for the pH 7 and pH 9 data were between 400–500 nm. The error bars in panel A are set at 10% of the measured value based on potential measurement error of the initial sample length. The error bars in panel B are calculated according to the propagation of error analysis detailed in the ESI.†

modulus values difficult to calculate. The same behavior occurred for both samples at pH 7, requiring high strain to be applied before wrinkles were formed (Fig. S13, ESI†). To address this, only the wrinkles that spanned across two cracks were used rather than the short wrinkles that only appeared at the periphery of the cracks (Fig. S12, ESI†). The salt screening and rearrangement of ionic pairing after salt annealing and rinsing caused an increased lateral and perpendicular diffusion of the polyelectrolytes.[19,43] The inhibited formation of wrinkles and cracking (*i.e.*, enhanced elongation at break) in these salt-annealed PEMs is attributed to an increased ductility caused by the exposure to salt solutions.

In contrast to SPAMA/SPMAA system, the LPAMA/LPMAA PEMs assembled at pH 5 formed cracks and wrinkles under low strain (5% strain, Fig. 7A) under the same salt annealing conditions as SPAMA/SPMAA. The higher ductility of SPAMA/SPMAA PEMs assembled from pH 5 than LPAMA/LPMAA PEMs correlates with a higher salt-induced diffusivity of the star polymers within the films, which agrees with previous reports of star PEMs.[40,42,43]

Lastly, Young's modulus values before and after salt annealing, shown in Fig. 7B, did not appear to change significantly for nearly all films except SPAMA/SPMAA at assembly pH 9. However, it is critical to note that the SIEBIMM technique is accurate at low strain, typically $<10\%$, so the Young's modulus values calculated at strains above 10% should be considered with some hesitancy. In the SIEBIMM equation (see Materials and methods), we assume that the PEM film is glassy, with a Poisson's ratio (ν_f) of 0.33, but this assumption may not hold true in the salt-annealed conditions. If the Poisson's ratio increases, *i.e.*, the film deforms more significantly in response to perpendicular applied strain, the calculated Young's modulus would in fact decrease from what is shown. The resulting increase in compliance may also necessitate the higher strain required to form wrinkles.

Yet, while Young's modulus and ductility often change together, it is possible for the PEM to become more ductile without compromising the stiffness. We suggest that in the salt-annealed SPAMA/SPMAA PEMs assembled from pH 5, where the ductility increases significantly but the stiffness remains similar, the ionic screening may promote some reorganization of the multilayers, increasing the film's ability to deform, without significantly changing its initial network of ionic and hydrogen-bonded pairs. Yet, the reduced modulus for the star PEMs assembled at pH 9 correlates well with the high sensitivity of star-containing-films to exposure to salt solutions.[40,42,43] These results show that salt annealing can be used to increase ductility while potentially maintaining the stiffness of the PEM films, particularly in star-containing films assembled from acidic conditions.

Conclusions

In this paper, we compared the growth, ionization, swelling, and mechanical properties of all-linear *versus* all-star (8-arm) weak PEM films assembled from PAMA and PMAA under varying assembly pH conditions. Our findings revealed that the growth and ionization characteristics of these PEMs are influenced by the assembly pH, with minimal impact of the polymer architecture. Notably, films assembled in acidic conditions, where PMAA has low ionization, exhibited slow, linear growth and generally higher Young's moduli compared to those assembled at neutral or slightly alkaline conditions, where nonlinear growth occurred.

However, when assembled from neutral or slightly alkaline conditions, the impact of polymer architecture was more pronounced in the swelling ratio and Young's modulus of the PEMs. Films containing star polyelectrolytes were stiffer and demonstrated more robust mechanical behavior as compared to their all-linear counterparts, including thickness- and pH-independent swelling and Young's modulus, as well as higher Young's modulus values. Lastly, we show that salt annealing the PEM films led to an increased ductility, and this effect was the most pronounced in films containing star polyelectrolytes.

Experimental

Materials

Linear PAMA, 8-arm PAMA, linear PMAA, and 8-arm PMAA (denoted LPAMA, SPAMA, LPMAA, and SPMAA, respectively) were synthesized as described previously.[43,44] The molecular weights of PMAAs were calculated from the number of monomer units provided in our previous work,[43] with LPMAA containing 695 monomer units (60 kDa) and SPMAA containing 767 monomer units (66 kDa). The molecular weights of PAMAs were calculated from the degree of polymerization provided in our previous work,[44] with LPAMA containing 310 monomer units (40 kDa) and SPAMA containing 320 monomer units (41 kDa).

Sodium phosphate monobasic dihydrate, hydrochloric acid, sodium hydroxide, and branched poly(ethylenimine) (750 kDa; Sigma-Aldrich, Saint Louis, MO, USA) were used as received. Silicon wafers (University Wafer, Inc., South Boston, MA, USA; ⟨100⟩ orientation, undoped, 0–100 Ω cm resistivity) and polydimethylsiloxane (PDMS; cured from Sylgard 184 Silicone Elastomer Kit Clear; Dow Chemical Company, Midland, MI, USA) were used as substrates for multilayer deposition. Ultrapure Milli-Q water (MilliporeSigma, Burlington, MA, USA) with a resistivity of 18.2 MΩ cm was used in all LbL experiments.

Substrate preparation

To prepare the substrates for layer-by-layer (LbL) deposition of PAMA and PMAA, PDMS substrates were cured from a 10 : 1 mixing ratio of elastomer base to curing agent by volume. The mixture was poured into lids of Petri dishes to about 2 mm thick and placed flat under vacuum for 30 min to remove any contained air bubbles. The mixture was then cured at 25 °C and ambient pressure for at least 24 h, and the cured PDMS was cut into 0.5 cm × 3 cm × 2 mm substrates. For basic characterization (*i.e.*, ellipsometric growth curves and infrared

spectroscopic analysis), undoped silicon wafers were cut into 1 cm × 1 cm squares and cleaned under ultraviolet light for at least 8 h.

Then, the silicon and PDMS substrates were cleaned by exposure to high RF level plasma generated from room-temperature ambient air for 60 s (Basic Plasma Cleaner PDC-32G 115V, Harrick Plasma, Ithaca, NY, USA) to remove organic contaminants and generate negatively charged silanol groups on the surface.

Layer-by-layer (LbL) film deposition

All solutions used for LbL deposition, *i.e.*, phosphate buffer (PB) rinses (0.01 M), LPAMA, LPMAA, SPAMA, and SPMAA (all 0.2 mg mL^{-1} in 0.01 M PB) were adjusted to pH 3, 5, 7, 9, or 11 by additions of 0.1 or 0.01 M NaOH or HCl. All polyelectrolyte solutions were left to dissolve overnight and filtered once with 0.45 um PTFE syringe filters (Scientific Strategies, LLC, Rush Springs, OK, USA) to remove dust and contaminants before LbL deposition.

Prior to the deposition of LbL films, the substrates were removed from the plasma cleaner (see prior section on Substrate preparation), immediately placed in a BPEI solution (0.2 mg mL^{-1} in Milli-Q water, adjusted to pH 9) for 45 min to prime the substrates with a monolayer of positively charged BPEI, and rinsed with 0.01 M PB at the specified pH of the deposition (*i.e.*, pH 3, 5, 7, 9, or 11). This priming step also functions to standardize the surface of the silicon wafers and PDMS substrates for further deposition.

To construct the growth curves for each pH, BPEI-primed silicon wafers were manually dipped into LPMAA or SPMAA solutions for 5 min and rinsed thoroughly in PB solution for 30 s to build the full 'prime bilayer', *i.e.*, the thickness at '0 bilayers' in the growth curves. To continue the growth curves, the silicon wafer was dipped into LPAMA or SPAMA solutions for 5 min, rinsed thoroughly in PB solution for 30 s, dipped into LPMAA or SPMAA for 5 min, and rinsed again in PB solution for 30 s to complete a bilayer. This process was repeated, and the dry film thickness was measured every two or five bilayers *via* spectroscopic ellipsometry.

For SIEBIMM experiments, the PAMA/PMAA multilayers were deposited on BPEI-primed PDMS substrates using a dipping robot (DR-3 Table Top Dipping Device, Riegler & Kirstein GmbH, Potsdam, Germany). For all PAMA/PMAA films, the PDMS substrates were held vertically in tweezers to be first dipped into the LPMAA or SPMAA solutions for 5 min and withdrawn at a speed of 1 cm s^{-1}, followed by two PB rinsing steps (10 fast dips in both rinse beakers), then dipped into LPAMA or SPAMA solutions for 5 min and withdrawn at a speed of 1 cm s^{-1}, followed by two PB rinsing steps (10 fast dips in both rinse beakers). This process was repeated until the desired film thickness as determined by spectroscopic ellipsometry. All films were capped with either LPMAA or SPMAA.

Comparing our thickness measurements with matched bilayer numbers between manual deposition on silicon and robot deposition on PDMS, we saw differences in thickness of about 10%, with thicker deposition using the robot on PDMS.

Ellipsometry

Measurements of the thickness and refractive index of the PAMA/PMAA LbL films on either silicon or PDMS substrates were characterized using a M-2000 automated-angle spectroscopic ellipsometer with CompleteEASE software (J. A. Woollam Co., Inc., Lincoln, NE, USA). Dry film measurements were collected at three different locations and at four incidence angles: 45, 55, 65, and 75°. To fit the ellipsometric data on silicon wafers, the dry polymer film on the wafer was treated as a graded layer of Cauchy material with the thickness d atop a silicon and native oxide layer. For measurements on PDMS substrates, treated as a graded layer of Cauchy material with the thickness d atop a Cauchy substrate (A = 1.400, B = 0.00433, C = 0.000). Fitting coefficients and thickness d were fitted simultaneously.

Swelling data were collected from PEMs deposited on silicon wafers and attached to glass slides using thermal glue. Prior to filling the wet cell with pH adjusted PB, the dry film thickness was measured in the cell for an accurate calculation of the swollen thickness. *In situ* ellipsometric measurements were taken at 75° until a constant swollen thickness was reached (~30 min). Wet-cell measurements of swollen polymer films required the addition of a fourth layer to the model to account for the refractive index of the solvent.

Attenuated total reflection – Fourier transform infrared (ATR-FTIR) spectroscopy

A Bruker Tensor II spectrometer equipped with a mercury cadmium telluride detector and an ATR diamond crystal (Bruker Optik GmbH, Ettlingen, Germany) was used for collecting ATR-FTIR spectra. The spectra were obtained with 96 scans in the 500–4000 cm^{-1} spectral range with a resolution of 2 cm^{-1}.

For peak identification, a monolayer of LPAMA, SPAMA, LPMAA and SPMAA (dissolved in ultrapure water) was deposited on a diamond ATR crystal by solution evaporation, and an infrared spectrum was collected under a constant stream of nitrogen gas to inhibit water absorption from the air. Relevant peaks were identified and deconvoluted in ImageJ.

The IR spectra of the LbL films were collected from PAMA/PMAA films deposited on undoped silicon wafers from pH 3, 5, 7, and 9 (>200 nm to increase sensitivity). To calculate the degree of ionization of PMAA within the films, the following equation was used.

$$\%_{\text{ion.}} = \frac{\text{Absorbance}_{1550\,\text{cm}^{-1}}}{\text{Absorbance}_{1700\,\text{cm}^{-1}} + \text{Absorbance}_{1550\,\text{cm}^{-1}}} \times 100\%$$

To calculate the percentage of PAMA within the films, the following equation was used

$$\%_{\text{PAMA}} = \frac{\text{Abs.}_{1720\,\text{cm}^{-1}}}{\text{Abs.}_{1720\,\text{cm}^{-1}} + \text{Abs.}_{1700\,\text{cm}^{-1}} + \text{Abs.}_{1550\,\text{cm}^{-1}}} \times 100\%$$

To calculate the relative percentage of water within the films, the following equation was used.

$$\%_{water} = \frac{Abs._{1640\,cm^{-1}}}{Abs._{1720\,cm^{-1}} + Abs._{1700\,cm^{-1}} + Abs._{1640\,cm^{-1}} + Abs._{1550\,cm^{-1}}} \times 100\%$$

Strain-induced elastic buckling for instability mechanical measurements (SIEBIMM) on LPAMA/LPMAA and SPAMA/SPMAA LbL films

To analyze the Young's modulus of the LbL coatings, the strain-induced elastic buckling instability for mechanical measurements (SIEBIMM) method was used. LbL coatings were deposited on PDMS substrates at various thicknesses.

In the SIEBIMM technique, a low mechanical strain is applied to the coated PDMS inducing 'wrinkles' with measurable buckling wavelengths that are used to determine the Young's modulus of the thin film, following the equation:

$$E_f = \frac{3E_s(1-\nu_f^2)}{1-\nu_s^2}\left(\frac{\lambda}{2\pi d_f}\right)^3$$

where E_f and E_s are Young's moduli of the film and substrate, respectively; ν_f and ν_s are Poisson's ratio of the film and substrate, respectively; λ is the buckling wavelength; and d_f is the film thickness. In the case of polyelectrolyte multilayers, the Poisson's ratio of dry PEM films (ν_f) is typically assumed to be 0.33.[27,29,61] Also, the Poisson's ratio for the PDMS (ν_s) was 0.5, and the Young's modulus of PDMS (E_s) was 1.75 MPa, as found by uniaxial tensile testing (ASTM D638).

Following a previously reported procedure for the SIEBIMM method on LbL-coated PDMS, the samples were subjected to a strain rate on the order of 10^{-4} s^{-1} up to 10–15% strain using a tensile stage (Kammrath & Weiss Tensile/Compression Module, 500 N) to determine the buckling wavelength, λ. The formation of wrinkles parallel to the direction of strain was imaged using a stereo microscope at 90× magnification (Olympus SZ51 with WHSZ15X eyepieces, a 110AL1.5X auxiliary objective, and SZ2-ILST stand). The buckling wavelengths of the wrinkles were analyzed in ImageJ from three images per samples (see ESI† for a detailed image analysis procedure).

Salt annealing of PEM films

PAMA/PMAA PEM films were exposed to 0.5 M NaCl solutions at matched pH values as assembly for 30 min, then thoroughly rinsed in phosphate buffer (no NaCl) at matched pH and dried under a gentle flow of nitrogen gas. The films remained at the surface in all cases except LPAMA/LPMAA pH 3, which lost nearly 90% of its original thickness. Because of the film removal at pH 3, we only tested the effect of salt-annealing on PEMs assembled from pH 5, 7, and 9.

Author contributions

Conceptualization – J. B., A. A., S. A. S.; formal analysis – J. B., A. L.; funding acquisition – S. A. S.; investigation – J. B., A. L., A. A.; methodology – J. B., A. A., S. A. S.; project administration – S. A. S.; visualization – J. B., S. A. S.; writing – original draft – J. B., A. L., A. A., S. A. S.; writing – review & editing – J. B., A. L., A. A., S. A. S. All authors have read and agreed to the published version of the manuscript.

Conflicts of interest

There are no conflicts to declare.

Data availability

The data supporting this article have been included as part of the ESI.†

Acknowledgements

This work was supported by the National Science Foundation under Award No. DMR-1905535 (S. A. S.). J. B. acknowledges support from the National Science Foundation Graduate Research Fellowship Program. Use of the Materials Characterization Facility at Texas A&M University is acknowledged.

References

1 J. J. Richardson, J. Cui, M. Björnmalm, J. A. Braunger, H. Ejima and F. Caruso, *Chem. Rev.*, 2016, **116**, 14828–14867.
2 B. M. Wohl and J. F. J. Engbersen, *J. Controlled Release*, 2012, **158**, 2–14.
3 S. Zhao, F. Caruso, L. Dähne, G. Decher, B. G. De Geest, J. Fan, N. Feliu, Y. Gogotsi, P. T. Hammond, M. C. Hersam, A. Khademhosseini, N. Kotov, S. Leporatti, Y. Li, F. Lisdat, L. M. Liz-Marzán, S. Moya, P. Mulvaney, A. L. Rogach, S. Roy, D. G. Shchukin, A. G. Skirtach, M. M. Stevens, G. B. Sukhorukov, P. S. Weiss, Z. Yue, D. Zhu and W. J. Parak, *ACS Nano*, 2019, **13**, 6151–6169.
4 P. T. Hammond, *Mater. Today*, 2012, **15**, 196–206.
5 L.-M. Petrila, F. Bucatariu, M. Mihai and C. Teodosiu, *Materials*, 2021, **14**, 4152.
6 L. Séon, P. Lavalle, P. Schaaf and F. Boulmedais, *Langmuir*, 2015, **31**, 12856–12872.
7 S. Guo, X. Zhu and X. J. Loh, *Mater. Sci. Eng. C*, 2017, **70**, 1163–1175.
8 H. Chang, H. Zhang, M. Hu, X.-C. Chen, K.-F. Ren, J.-L. Wang and J. Ji, *Biomater. Sci.*, 2015, **3**, 352–360.
9 J. M. Silva, J. R. García, R. L. Reis, A. J. García and J. F. Mano, *Acta Biomater.*, 2017, **51**, 279–293.
10 E. Kharlampieva and S. A. Sukhishvili, *Langmuir*, 2003, **19**, 1235–1243.
11 S. T. Dubas and J. B. Schlenoff, *Macromolecules*, 2001, **34**, 3736–3740.
12 J. Choi and M. F. Rubner, *Macromolecules*, 2005, **38**, 116–124.
13 L. Xu, D. Pristinski, A. Zhuk, C. Stoddart, J. F. Ankner and S. A. Sukhishvili, *Macromolecules*, 2012, **45**, 3892–3901.

14 V. Izumrudov and S. A. Sukhishvili, *Langmuir*, 2003, **19**, 5188–5191.
15 S. T. Dubas and J. B. Schlenoff, *Macromolecules*, 1999, **32**, 8153–8160.
16 J. B. Schlenoff and S. T. Dubas, *Macromolecules*, 2001, **34**, 592–598.
17 J. F. Quinn and F. Caruso, *Langmuir*, 2004, **20**, 20–22.
18 J. Campbell and A. S. Vikulina, *Polymers*, 2020, **12**, 1949.
19 V. Selin, J. F. Ankner and S. A. Sukhishvili, *Macromolecules*, 2015, **48**, 3983–3990.
20 G. Decher, *Science*, 1997, **277**, 1232–1237.
21 M. T. Thompson, M. C. Berg, I. S. Tobias, M. F. Rubner and K. J. Van Vliet, *Biomaterials*, 2005, **26**, 6836–6845.
22 P. V. Pavoor, A. Bellare, A. Strom, D. Yang and R. E. Cohen, *Macromolecules*, 2004, **37**, 4865–4871.
23 O. Mermut, J. Lefebvre, D. G. Gray and C. J. Barrett, *Macromolecules*, 2003, **36**, 8819–8824.
24 R. Hlushko, J. F. Ankner and S. A. Sukhishvili, *Macromolecules*, 2020, **53**, 1033–1042.
25 C. M. Stafford, C. Harrison, K. L. Beers, A. Karim, E. J. Amis, M. R. Vanlandingham, H.-C. Kim, W. Volksen, R. D. Miller and E. E. Simonyi, *Nat. Mater.*, 2004, **3**, 545–550.
26 J. Y. Chung, A. J. Nolte and C. M. Stafford, *Adv. Mater.*, 2011, **23**, 349–368.
27 A. J. Nolte, M. F. Rubner and R. E. Cohen, *Macromolecules*, 2005, **38**, 5367–5370.
28 E. Niinivaara, J. Desmaisons, A. Dufresne, J. Bras and E. D. Cranston, *J. Colloid Interface Sci.*, 2021, **582**, 227–235.
29 A. J. Nolte, R. E. Cohen and M. F. Rubner, *Macromolecules*, 2006, **39**, 4841–4847.
30 L. Xu, V. Kozlovskaya, E. Kharlampieva, J. F. Ankner and S. A. Sukhishvili, *ACS Macro Lett.*, 2012, **1**, 127–130.
31 G. Ladam, P. Schaad, J. C. Voegel, P. Schaaf, G. Decher and F. Cuisinier, *Langmuir*, 2000, **16**, 1249–1255.
32 C. Porcel, P. Lavalle, V. Ball, G. Decher, B. Senger, J.-C. Voegel and P. Schaaf, *Langmuir*, 2006, **22**, 4376–4383.
33 P. Bieker and M. Schönhoff, *Macromolecules*, 2010, **43**, 5052–5059.
34 P. Nestler, M. Paßvogel and C. A. Helm, *Macromolecules*, 2013, **46**, 5622–5629.
35 A. Azinfar and C. A. Helm, *Macromolecules*, 2023, **56**, 3095–3109.
36 K. C. Stevens and M. V. Tirrell, *ACS Macro Lett.*, 2024, **13**, 688–694.
37 I. Choi, R. Suntivich, F. A. Plamper, C. V. Synatschke, A. H. E. Müller and V. V. Tsukruk, *J. Am. Chem. Soc.*, 2011, **133**, 9592–9606.
38 B. Mendrek, N. Oleszko-Torbus, P. Teper and A. Kowalczuk, *Prog. Polym. Sci.*, 2023, **139**, 101657.
39 A. Chremos, C. Jeong and J. F. Douglas, *Soft Matter*, 2017, **13**, 5778–5784.
40 A. Aliakseyeu, J. F. Ankner and S. A. Sukhishvili, *Macromolecules*, 2022, **55**, 8150–8161.
41 B.-S. Kim, H. Gao, A. A. Argun, K. Matyjaszewski and P. T. Hammond, *Macromolecules*, 2009, **42**, 368–375.
42 J. Brito, P. P. Shah, A. Aliakseyeu and S. A. Sukhishvili, *J. Chem. Phys.*, 2024, **160**, 121101.
43 A. Aliakseyeu, P. P. Shah, J. F. Ankner and S. A. Sukhishvili, *Macromolecules*, 2023, **56**, 5434–5445.
44 A. Aliakseyeu, R. Hlushko and S. A. Sukhishvili, *Polym. Chem.*, 2022, **13**, 2637–2650.
45 K. L. Thompson, E. S. Read and S. P. Armes, *Polym. Degrad. Stab.*, 2008, **93**, 1460–1466.
46 N. G. Hoogeveen, M. A. C. Stuart, G. J. Fleer, W. Frank and M. Arnold, *Macromol. Chem. Phys.*, 1996, **197**, 2553–2564.
47 J. Dong, N. Tsubahara, Y. Fujimoto, Y. Ozaki and K. Nakashima, *Appl. Spectrosc.*, 2001, **55**, 1603–1609.
48 S. A. Sukhishvili and S. Granick, *Macromolecules*, 2002, **35**, 301–310.
49 T. Mauser, C. Déjugnat and G. B. Sukhorukov, *Macromol. Rapid Commun.*, 2004, **25**, 1781–1785.
50 S. E. Burke and C. J. Barrett, *Biomacromolecules*, 2003, **4**, 1773–1783.
51 K. Itano, J. Choi and M. F. Rubner, *Macromolecules*, 2005, **38**, 3450–3460.
52 T. Alonso, J. Irigoyen, J. J. Iturri, I. L. Larena and S. E. Moya, *Soft Matter*, 2013, **9**, 1920–1928.
53 A. Jaklenec, A. C. Anselmo, J. Hong, A. J. Vegas, M. Kozminsky, R. Langer, P. T. Hammond and D. G. Anderson, *ACS Appl. Mater. Interfaces*, 2016, **8**, 2255–2261.
54 S. S. Shiratori and M. F. Rubner, *Macromolecules*, 2000, **33**, 4213–4219.
55 J. Fu, H. M. Fares and J. B. Schlenoff, *Macromolecules*, 2017, **50**, 1066–1074.
56 L. A. Connal, Q. Li, J. F. Quinn, E. Tjipto, F. Caruso and G. G. Qiao, *Macromolecules*, 2008, **41**, 2620–2626.
57 H. H. Rmaile and J. B. Schlenoff, *Langmuir*, 2002, **18**, 8263–8265.
58 J. D. Mendelsohn, C. J. Barrett, V. V. Chan, A. J. Pal, A. M. Mayes and M. F. Rubner, *Langmuir*, 2000, **16**, 5017–5023.
59 A. I. Petrov, A. A. Antipov and G. B. Sukhorukov, *Macromolecules*, 2003, **36**, 10079–10086.
60 S. E. Burke and C. J. Barrett, *Langmuir*, 2003, **19**, 3297–3303.
61 A. J. Nolte, N. D. Treat, R. E. Cohen and M. F. Rubner, *Macromolecules*, 2008, **41**, 5793–5798.
62 E. Kharlampieva, V. Kozlovskaya, J. F. Ankner and S. A. Sukhishvili, *Langmuir*, 2008, **24**, 11346–11349.
63 L. Xu, J. F. Ankner and S. A. Sukhishvili, *Macromolecules*, 2011, **44**, 6518–6524.